*J Mater Sci* (2025) 60:8536–8544

Metals & corrosion

# Mössbauer characterisation of bearing steels and dark etching regions

Sebastián Echeverri Restrepo[1,2,*], Hanzheng Huang[1,3], Mohamed Y. Sherif[1], and A. Iulian Dugulan[4]

[1] SKF Research and Technology Development (RTD), SKF B.V, Meidoornkade 14, 3992 AE Houten, The Netherlands
[2] Department of Physics, King's College London, Strand, London WC2R 2LS, United Kingdom
[3] Department of Materials Science and Engineering, Delft University of Technology, Mekelweg 2, 2628 CD Delft, The Netherlands
[4] Fundamental Aspects of Materials and Energy Group, Delft University of Technology, Mekelweg 15, 2629 JB Delft, The Netherlands

**Received:** 29 January 2025
**Accepted:** 22 April 2025
**Published online:** 20 May 2025



## ABSTRACT

Dark etching regions (DERs) are a widely studied phenomenon in the context of sub-surface microstructure decay in rolling bearings. These regions result from dislocation motion (plasticity) and carbon migration due to rolling contact fatigue (RCF). We conducted a systematic study using Mössbauer spectroscopy to identify phase evolution during tempering and DER formation. Our findings resolve a long-standing debate in the literature by demonstrating that fine temper carbides dissolve during DER formation. A slight decrease in non-stoichiometric carbides was observed in the DERs, indicating the dissolution of fine carbides. The released carbon is believed to back-diffuse into ferrite and/or martensite.

## Introduction

The classic 1% carbon–1.5% chromium bearing steel (ASTM A295 52100, we will refer to it as ASTM 52100 in the rest of the article) is the most common bearing steel and has existed for over 100 years in the bearing industry. This steel is often martensitically through hardened by heating it to a high temperature, followed by quenching and tempering. The resulting homogenous microstructure, containing tempered martensite, retained austenite and carbides (coarse and fine), offers the hardness and toughness levels required in bearing applications.

When bearing steel is subjected to rolling contact fatigue (RCF), its microstructure decays; the phases that are initially present are (partially) transformed and some new ones emerge. One of the microstructural changes which occurs in bearings during RCF that has been widely reported in the literature is the formation of sub-surface dark etching regions (DERs) [1–11].

In general, there is consensus about the changes that the initial microstructure suffers during the formation of DERs. The martensitic matrix decays, the available retained austenite transforms into martensite, the coarse residual carbides—undissolved during austenitisation—remain unaltered, and there is an extensive redistribution of carbon. The remaining question is whether the fine carbides, initially formed through tempering, dissolve or grow as DERs develop..

Handling Editor: Sophie Primig.

Address correspondence to E-mail: Sebastian.Echeverri.Restrepo@skf.com


https://doi.org/10.1007/s10853-025-10930-6

Fine temper carbides, present in the form of transition carbides or temper cementite, precipitate in a typical bearing steel at the later stages of the heat treatment, during low-temperature tempering at 160 °C to 270 °C [1, 11]. They play an important role in the RCF behaviour of bearing steels; through the mechanism of precipitation hardening, they impede the free movement of dislocations, contributing to the good fatigue performance of the tempered material [2].

With respect to the evolution of the fine temper carbides during the formation of DERs, two main schools of thought have surfaced since the middle of the twentieth century, when the microstructural alterations caused by RCF began to be studied (see e.g. [3, 12–20]). These two schools of thought have opposite views: the first one claims that the fine temper carbides dissolve, while the second one claims that they tend to coarsen.

Advocates of the dissolution theory propose a stress-induced break-up mechanism that generates a net carbon flux from the temper carbides [5] towards existing dislocations [4]. Others suggest that there is a gradual dissolution of the temper carbides, driven by carbon segregation towards initially pinned dislocations which bow under the stresses generated by RCF [2]. In contrast, supporters of the coarsening theory argue that the initial martensite is transformed into polygonal structures with fine precipitates surrounding them [21], or that the DERs correspond to ferrite and fine carbides [22]. It is not clear if these fine carbides/precipitates belong to the initial temper carbides or to a newly precipitated set. More recently, it has been proposed that, during DER formation, the carbon present in the matrix migrates to pre-existing carbide precipitates, assisted by the glide of dislocations [10, 23].

Common techniques previously used for the characterisation of DERs include X-ray diffraction (XRD), transmission electron microscopy (TEM), and atom probe tomography (APT), each one having its own advantages and disadvantages. With TEM and APT it is possible to focus on small regions and locate individual temper carbides. While with TEM one can get information about their crystalline structure and composition, with APT a detailed characterisation of individual carbides is not evident. On the other hand, while APT allows the investigation of the distribution of atomic carbon in the matrix, TEM does not. Perhaps the main limitation of both techniques is the small size of the region that can be analysed; it is not possible to get statistically relevant information about the global microstructural changes in the phase fractions and their corresponding carbon concentration. XRD has the advantage that it can analyse relatively large regions, but it is not useful for the indexation of small carbides, making it difficult to obtain reliable quantification of the carbide fractions in the microstructure. It also does not allow to study local changes in carbon concentrations.

An alternative technique, until now not used for the characterisation of temper carbides in bearing steels, is Mössbauer spectroscopy. It allows to study statistically relevant regions, while being precise enough to identify the structure of temper carbides, the phase fractions in the microstructure, and the changes on the concentration of carbon in the matrix. In Mössbauer spectroscopy, signals are measured from individual Fe atoms, allowing the fitted spectral contributions to be directly related to the mole fractions of different Fe species. No Fe atoms are silent to Mössbauer spectroscopy; even mono-atomically dispersed Fe species are detectable.

In the present work, we aim to solve this dissolution versus coarsening dispute by studying the evolution of phase fractions and carbon migration during DER formation in martensitic-hardened ASTM 52100 steel using, for the first time, Mössbauer spectroscopy.

## Methods

### Sample preparation

Two types of samples were considered. The first type, reference samples, were custom made to calibrate and distinguish the response of individual microstructural constituents to Mössbauer spectroscopy. They contain reference structures with distinct populations of phases. The second type, DER samples, are directly taken from bearing rings previously subjected to RCF, containing DERs (a cross section of a bearing inner ring with DERs is presented in Fig. 1 ). All the samples used for this study were made from bearing steel ASTM 52100 (see composition in Table 1).

#### *Reference samples*

For the reference samples, four sets of samples, 25mm in diameter and 10mm thick, were produced and heat treated by austenitisation, quenching in oil, and

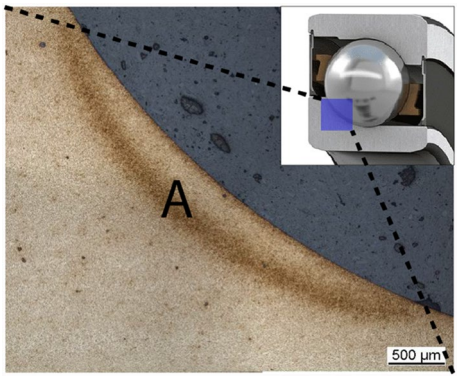


**Figure 1** Light optical microscopy image of the cross section of the bearing (SKF 7209 BECBP) inner ring used for the extraction of samples. DER samples were taken from region A. The insert on the top right corner shows a bearing (sectioned). The micrograph was taken from the area highlighted in blue (not including the ball).

**Table 1** Chemical composition of ASTM 52100 bearing steel in wt%

| | | | | |
|---|---|---|---|---|
| C | Mn | P | S | Si |
| 0.93–1.05 | 0.25–0.45 | ≤ 0.025 | ≤ 0.015 | 0.15–0.35 |
| Ni | Cr | Cu | Mo | |
| ≤ 0.25 | 1.35–1.60 | ≤ 0.30 | ≤ 0.10 | |

tempering. The tempering step –if applicable– was varied between the samples as follows: Samples T0 were left untempered, while samples T1 and T2 were immediately tempered at 160 °C for 90 min, and 220 °C for 4 h, respectively. The final set of samples, T3, were promptly stabilised at 350 °C for 4 h. For the Mössbauer measurements, slices of 0.1mm were cut and their thickness was further reduced to ≈ 50µm via mechanical polishing. T2 corresponds to the microstructure where the DERs were formed.

The untempered state (T0) was designed to prevent transition carbides from forming. Tempering at the intermediate temperatures of 160 °C and 220 °C (T1 and T2, respectively) was expected to yield transition carbides, whereas stabilisation (T3) was carried out at sufficiently high temperature for transition carbides to convert into the more thermodynamically stable cementite [24].

### *DER samples*

For the study of the DERs, samples were extracted from bearing rings after endurance tests lasting for $18.14 \times 10^6$ and $22.66 \times 10^6$ revolutions. We will refer to the samples as DER I and DER II, respectively. The tests were performed with an axial load of 50KN at a rotational speed of 6000 RPM and a constant outer ring temperature of 75 °C.

Thin slices of approximately 0.5mm thickness were cut from the cross section of the bearing ring and mechanically polished to further reduce their thickness to around 100µm. Each polished slice was then etched using 1.5 wt% Nital, revealing the DERs. Regions with DER were identified and punched out using a GATAN 3mm disc punch, a tool designed for transmission electron microscopy sample preparation. Approximately 20 pieces of these punched-out samples were collected for subsequent Mössbauer spectroscopy characterisation.

A schematic view of the process of sample preparation is presented in Fig. 2.

## Mössbauer spectroscopy

Mössbauer spectroscopy is a resonant gamma-ray absorption technique that measures hyperfine interactions between electrons and nuclei with an accuracy of 13–15 orders of magnitude [25]. It is widely recognised for its unparalleled resolution among spectroscopic techniques [26].

In the present work, transmission $^{57}$Fe Mössbauer spectra[1] were collected at 295K (22 °C) with a conventional constant-acceleration spectrometer using a $^{57}$Co(Rh) source. Velocity calibration was carried out using an $\alpha$-Fe foil. The Mössbauer spectra, together with the corresponding uncertainties, were fitted and calculated using the software Mosswinn 4.0 [27], in transmission integral mode (accounting for saturation effects).

The following coding is used when displaying the results of the measured Mössbauer spectra. The red lines represent the raw measured data and the total fitted spectrum. The other fitted contributions, or subspectra, are shown in different colours and can exhibit one peak (for cubic symmetry paramagnetic species),

[1] All the Mössbauer spectroscopy measurements were done at the TU Delft Reactor Institute.

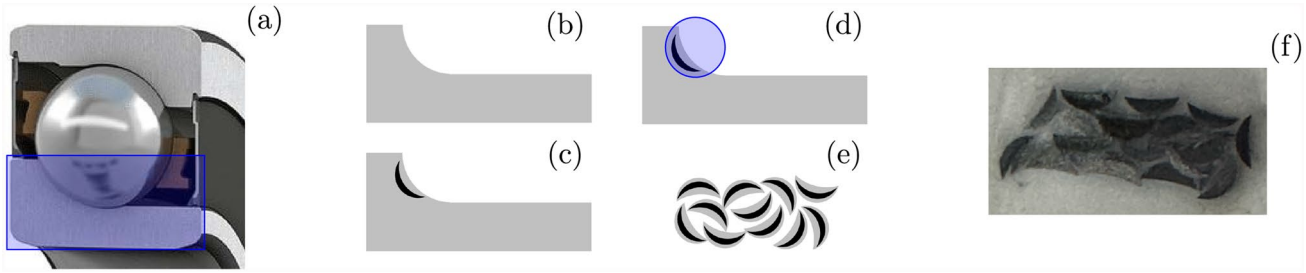


**Figure 2** Schematic view of the process followed for the preparation of the DER I and DER II sample clusters to make them suitable for Mössbauer measurements. **a** Cross section of a bearing where the inner ring is highlighted. **b** Cut and polished thin slices from the cross section of the inner ring. **c** Polished slices to reveal the location of the DERs. **d** Moon-shaped regions containing DERs are punched out of the slices. **e** Clusters of moon-shaped regions are collected to form a sample suitable for Mössbauer measurements. **f** Cluster used for the Mössbauer measurements of DER II. A similar cluster was made for DER I.

two peaks (for paramagnetic structures with charge asymmetry), or six peaks (when a magnetic field is present at the Fe nuclei).

## Results

### Mössbauer characterisation

The Mössbauer spectra of the martensitic phase (Fig. 3, Table 2) were resolved using three ferromagnetic components assigned to 1) Fe atoms remote from interstitial carbon atoms ($Fe^0$), 2) Fe atoms with one next nearest carbon atom at an octahedral site ($Fe_{nnn}$) and 3) Fe atoms with one nearest carbon at an octahedral site ($Fe_{nn}$) [28]. We will use the spectral contributions to quantify the amount of each phase in the material. The spectral contribution of a given phase, in the case of this specific steel, corresponds to the atomic percentage of the total Fe atoms present in the given phase [29].

#### *Reference samples*

With regard to the reference untempered (T0) and (T1) tempered samples, a significant amount of retained austenite ($\gamma$-Fe(0)), ~13-14% of the spectra, was present, allowing a clear assignment of its Mössbauer spectral parameters—in line with the fitting procedure presented in [30]. The austenite spectral contribution ($\gamma$-Fe(0)) is significantly reduced after higher temperature tempering procedures (compare samples T0 and T1 with samples T2 and T3). Simultaneously, more

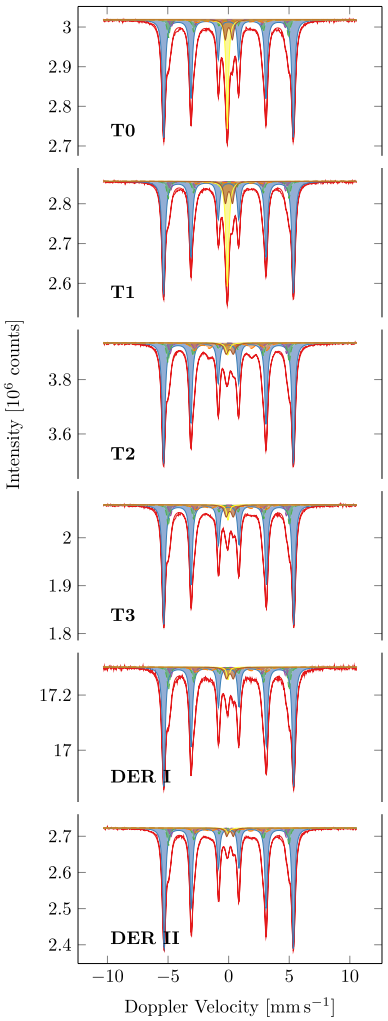


**Figure 3** Mössbauer spectra obtained at 295K (22 °C) with different tempered steel samples. The first four correspond to heat treatments T0, T1, T2 and T3. The last two correspond to the samples with dark etching regions (DER I and DER II).

**Table 2** Mössbauer fitted parameters for the steel samples

| Material | T (K) | IS (mm/s) | QS (mm/s) | Hyperfine field (T) | Phase | Spectral contribution (%) |
|---|---|---|---|---|---|---|
| T0 | 295 | 0.01 | 0.00 | 33.2 | $Fe^0$ | 63 ± 1.3 |
| | | 0.01 | 0.01 | 30.8 | $Fe_{nnn}$ | 10 ± 0.20 |
| | | 0.00 | 0.00 | 29.2 | $Fe_{nn}$ | 4 ± 0.08 |
| | | −0.08 | – | – | $\gamma$-Fe(0) | 13 ± 0.26 |
| | | 0.04 | 0.58 | - | $Fe_xC$ | 6 ± 0.12 |
| | | 0.18 | 0.00 | 17.4 | $\theta$-$Fe_3C$ | 4 ± 0.08 |
| T1 | 295 | 0.01 | 0.00 | 33.3 | $Fe^0$ | 61 ± 1.22 |
| | | 0.01 | 0.01 | 31.0 | $Fe_{nnn}$ | 9 ± 0.18 |
| | | 0.00 | 0.00 | 29.5 | $Fe_{nn}$ | 5 ± 0.10 |
| | | −0.08 | – | – | $\gamma$-Fe(0) | 14 ± 0.28 |
| | | 0.04 | 0.58 | – | $Fe_xC$ | 7 ± 0.14 |
| | | 0.21 | 0.00 | 17.1 | $\theta$-$Fe_3C$ | 4 ± 0.08 |
| T2 | 95 | 0.01 | 0.00 | 33.4 | $Fe^0$ | 68 ± 1.36 |
| | | 0.01 | 0.01 | 31.1 | $Fe_{nnn}$ | 12 ± 0.24 |
| | | 0.00 | 0.01 | 29.8 | $Fe_{nn}$ | 6 ± 0.12 |
| | | −0.05 | – | – | $\gamma$-Fe(0) | 2 ± 0.04 |
| | | 0.09 | 0.59 | – | $Fe_xC$ | 5 ± 0.10 |
| | | 0.18 | 0.00 | 17.9 | $\theta$-$Fe_3C$ | 7 ± 0.14 |
| T3 | 295 | 0.01 | 0.00 | 33.3 | $Fe^0$ | 67 ± 1.34 |
| | | 0.01 | 0.02 | 31.1 | $Fe_{nnn}$ | 11 ± 0.22 |
| | | 0.00 | 0.00 | 29.8 | $Fe_{nn}$ | 6 ± 0.12 |
| | | −0.06 | – | – | $\gamma$-Fe(0) | 2 ± 0.04 |
| | | 0.11 | 0.59 | – | $Fe_xC$ | 5 ± 0.10 |
| | | 0.16 | 0.00 | 18.5 | $\theta$-$Fe_3C$ | 9 ± 0.18 |

Experimental uncertainties: isomer shift (IS) ±0.01 mm/s; quadrupole splitting (QS) ±0.01 mm/s; hyperfine field ±0.1 T

ferromagnetic cementite is precipitating, its spectral contribution doubling in size.

The measured doublet with ~0.58 mm/s quadrupole splitting was assigned to a (super)paramagnetic carbide, $Fe_xC$, most likely non-stoichiometric cementite, highly dispersed into the ferrite structure. The presence of paramagnetic cementite at room temperature has been observed in previous studies [31–33]. The spectral contribution of better-defined ferromagnetic cementite ($\theta$-$Fe_3C$) detected in the samples (4% for T0 and T1, and 7% and 9% for T2 and T3, respectively) demonstrates the precipitation of cementite during tempering.

Carbon segregation with increased tempering intensity is also observed in the increasing field values of the ferromagnetic components. The partial withdrawal of carbon neighbours from the Fe vicinity, which are acting as magnetic diluents, leads to strengthening of the hyperfine field. This effect is better observed at the $Fe_{nn}$ site, where the hyperfine field value increases gradually from 29.2 T - 29.5 T - to 29.8 T for the samples T0, T1 and T2-T3, respectively.

### *DER samples*

The Mössbauer spectra obtained from the two DER samples (DER I and DER II) (Fig. 3) were fitted in a similar way, with main contributions from ferrite (hyperfine field ~33.3 T, 33.2 T) and two other components with decreased magnetic fields (31.0 T, 30.9 T and 29.5 T, 29.6 T), due to the presence of octahedral $Fe_{nnn}$ and $Fe_{nn}$ atoms. The presence of austenite and paramagnetic/ferromagnetic cementite

has also been observed in the spectra, the results being similar to those obtained with the stabilised sample (T3) (Table 3).

## Discussion

From the Mössbauer measurements, the amount of ferrite and martensite is given by the sum of three contributions, namely $Fe^0$, $Fe_{nnn}$ and $Fe_{nn}$; the amount of austenite is given by $\gamma$-Fe(0); and the amount of carbides by the sum of $Fe_xC$ and $\theta$-$Fe_3C$. For the case of T1, the measured ferrite and martensite is 75 %, the measured retained austenite is 14 %, and the measured amount of carbides is 11 %. In the same order, for T2, we get 86 %, 2 %, and 12 %; for T3, we get 84 %, 2 %, and 14 %. For T0, the contents are 77 %, 13 % and 10 %.

We obtain a reasonable agreement between the results obtained using Mössbauer spectroscopy and the expected phase fractions from the heat treatments, see Table 4. This is in line with previous literature, where Mössbauer spectroscopy has demonstrated great capability for the study and identification of carbides [34, 35].

As previously mentioned, by tempering sample T0 for 90 min at 160 °C we obtain sample T1, as evidenced by a slight increase from 6 to 7% on the spectral contribution of $Fe_xC$, indicating the formation of additional transition carbides. Longer tempering times at higher temperatures (samples T2 and T3) show a decrease of the spectral contribution of $Fe_xC$ to 5% and an increase of $\theta$-$Fe_3C$ by 3-5% compared to sample T1, showing that some of the transition carbides are no longer non-stoichiometric and have transformed into the more stable cementite. We also note that there is a global increase of the contribution of the carbides (transition+cementite), which is evidence that carbides are being formed and grow during the tempering process.

With regard to retained austenite, we note that, due to the shorter tempering time and lower temperature, there is essentially no change between the samples T0 and T1, the spectral contribution $\gamma$-Fe(0) remaining almost unchanged (13% vs 14%). As the tempering time is extended and the temperature increased, virtually all the austenite is transformed. The changes in the microstructure detected by Mössbauer are in good agreement with what is expected from the heat treatments applied to the different samples [24].

We remind the reader that T2 corresponds to the microstructure where the DERs were formed, so

**Table 4** Spectral contribution (%) of ferrite and martensite, austenite and carbides obtained using Mössbauer spectroscopy

| | Ferrite/martensite | Austenite | Carbides |
|---|---|---|---|
| T0 | 77 | 13 | 10 |
| T1 | 75 | 14 | 11 |
| T2 | 86 | 2 | 12 |
| T3 | 84 | 2 | 14 |

**Table 3** The Mössbauer fitted parameters of the steel samples with DER

| Material | T (K) | IS (mm/s) | QS (mm/s) | Hyperfine field (T) | Phase | Spectral contribution (%) |
|---|---|---|---|---|---|---|
| DER I | 295 | 0.01 | 0.00 | 33.3 | $Fe^0$ | 68 ± 1.36 |
| 18.14 | | 0.01 | 0.01 | 31.0 | $Fe_{nnn}$ | 13 ± 0.26 |
| Mrevs | | 0.00 | 0.01 | 29.5 | $Fe_{nn}$ | 6 ± 0.12 |
| | | −0.05 | – | – | $\gamma$-Fe(0) | 2 ± 0.04 |
| | | 0.10 | 0.56 | – | $Fe_xC$ | 4 ± 0.08 |
| | | 0.19 | 0.00 | 18.0 | $\theta$-$Fe_3C$ | 7 ± 0.14 |
| DER II | 295 | 0.01 | 0.00 | 33.2 | $Fe^0$ | 73 ± 1.46 |
| 22.66 | | 0.01 | 0.01 | 30.9 | $Fe_{nnn}$ | 11 ± 0.22 |
| Mrevs | | 0.00 | 0.00 | 29.6 | $Fe_{nn}$ | 5 ± 0.10 |
| | | −0.04 | – | – | $\gamma$-Fe(0) | 1 ± 0.02 |
| | | 0.11 | 0.54 | – | $Fe_xC$ | 3 ± 0.06 |
| | | 0.19 | 0.00 | 17.8 | $\theta$-$Fe_3C$ | 7 ± 0.14 |

Experimental uncertainties: isomer shift (IS) ±0.01 mm/s; quadrupole splitting (QS) ±0.01 mm/s; hyperfine field ±0.1 T

the discussion about the DERs will be focused on the microstructure of T2, and how it evolves during RCF to DER I (after 18.14 Mrevs) and DER II (after 22.66 Mrevs). The measurements show a slight increase of the spectral contribution of the three components that represent ferrite and martensite (sum of $Fe^0$, $Fe_{nnn}$ and $Fe_{nn}$); the joint contribution increases from 86 % to 87 % when going from T2 to DER I, and a further increase to 89 % when transitioning to DER II. This increase indicates that, during the formation of the DERs, there is flow of carbon towards the ferritic/martensitic phases. Since it is known that DERs are softer than the original microstructure [3, 36], we hypothesise that the carbon atoms migrate towards the grain boundaries of the newly formed ferrite and not to the centre of the grains, where they would cause hardening.

Interestingly, there is another small difference in the ferritic/martensitic components between the T2 and the two DER samples. The hyperfine fields at the three main ferromagnetic contributions ($Fe^0$, $Fe_{nnn}$ and $Fe_{nn}$) decrease slightly in the DER samples. This is best visible at the $Fe_{nn}$ site, where the hyperfine field decreases from 29.8 T to 29.5 T and 29.6 T, on T2, DER I and DER II, respectively. Carbon atoms appear to be pushed in the vicinity of the Fe atoms in the martensitic components, acting as magnetic diluents and thereby reducing the measured hyperfine field. This effect is opposite to that observed during the tempering process.

With respect to retained austenite, the Mössbauer measurements show a decrease from 2% to 1% of the $\gamma$-Fe(0) component during the formation of the DERs. Transformation of retained austenite is expected due to the fact that the microstructure is subjected to stress during RCF. Retained austenite transforms to the more stable ferritic/martensitic phases.[6, 37].

The spectral contribution of the $\theta$-$Fe_3C$ component remains constant during the formation of DERs. The value of 7% does not change in the T2, DER I and DER II samples, indicating that the amount of cementite does not change, consistent with previous observations available in the literature [21]. On the other hand, the spectral contribution $Fe_xC$, which represents the smaller transition non-stoichiometric carbides, is decreased during the formation of DERs. Their spectral contribution is reduced from 5 % in T2, to 4 % in DER I, to 3 % in DER II, a sign that there is a global dissolution of these type of carbides, and carbon back-diffusion to ferrite and/or martensite.

## Conclusions

The processes of tempering and DER formation in martensitic-hardened ASTM 52100 bearing steel were investigated using Mössbauer spectroscopy.

An increase of ferrite and/or martensite (86 % to 89%) and a decrease of austenite (2% to 1%) were observed in DERs, compared with the T2 microstructure. The hyperfine fields of $Fe_{nn}$ decrease (6% to 5%) in the DER samples, indicating carbon atoms being pushed in the vicinity of the Fe atoms in the martensitic components. This effect is opposite to that observed during the tempering process.

Mössbauer spectroscopy revealed two components of carbides, namely well-defined cementite and non-stoichiometric carbides. The phase fraction of non-stoichiometric carbides decreased during longer tempering times and higher temperatures, while the amount of well-defined cementite increased. After DER formation, the amount of well-defined cementite remained unaltered. A slight decrease of non-stoichiometric carbides was observed in DERs (5% to 4% to 3%), indicating dissolution of fine carbides during the RCF tests. The released carbon is believed to back-diffuse to ferrite and/or martensite. Since DERs are observed to soften relative to the as manufactured material, we hypothesise that the carbon atoms migrate towards the grain boundaries of the newly formed ferrite and not to the centre of the grains, where they would cause hardening.

## Acknowledgements

The authors would like to thank Aidan Kerrigan from SKF B. V. for his technical advice and for the thorough revision of the manuscript.

## Author Contributions

Sebastián Echeverri Restrepo contributed to conceptualisation, formal analysis, funding acquisition, investigation, methodology, project administration, resources, supervision, validation, visualisation, writing—original draft, and writing—review and editing. Hanzheng Huang was involved in formal analysis, investigation, methodology, supervision, validation, writing—original draft, and writing—review and editing. Mohamed Y. Sherif contributed

to conceptualisation, formal analysis, investigation, methodology, and writing—review and editing. Iulian Dugulan was responsible for conceptualisation, data curation, formal analysis, funding acquisition, investigation, methodology, resources, software, visualisation, writing—original draft, and writing—review and editing.

## Data Availability

The data used for this work will be made available upon reasonable request.

## Declarations

**Conflict of interest** The authors declare that there are no Conflict of interest regarding the publication of this article.

**Ethical Approval** Not Applicable

## References


[1] Bhadeshia HKDH (2012) Steels for bearings. Prog Mater Sci 57(2):268–435. https://doi.org/10.1016/j.pmatsci.2011.06.002

[2] Gegner J (2011) Tribological aspects of rolling bearing failures. In: Tribology - Lubricants and Lubrication. InTech. https://doi.org/10.5772/20790 . http://www.intechopen.com/books/tribology-lubricants-and-lubrication/tribological-aspects-of-rolling-bearing-failures

[3] Bush JJ, Grube WL, Robinson GH (1961) Microstructural and residual stress changes in hardened steel due to rolling contact. Trans. Amer. Soc. Metals 54:390–412818823

[4] Becker PC, Swahn H, Vingsbo O (1976) Structural changes in ball bearing steels caused by rolling contact fatigue. Mechanique matériaux électricité 320–321:8–14

[5] Swahn H, Becker PC, Vingsbo O (1976) Electron-microscope studies of carbide decay during contact fatigue in ball bearings. Metal Sci 10(1):35–39. https://doi.org/10.1179/030634576790431444

[6] Voskamp AP, Österlund R, Becker PC, Vingsbo O (1980) Gradual changes in residual stress and microstructure during contact fatigue in ball bearings. Metals Technol 7(1):14–21. https://doi.org/10.1179/030716980803286676

[7] Abdullah MU, Khan ZA, Kruhoeffer W (2020) Evaluation of dark etching regions for standard bearing steel under accelerated rolling contact fatigue. Tribol Int 152:106579. https://doi.org/10.1016/j.triboint.2020.106579

[8] El Laithy M, Wang L, Harvey TJ, Vierneusel B (2020) Re-investigation of dark etching regions and white etching bands in SAE 52100 bearing steel due to rolling contact fatigue. Int J Fatigue 136(March):105591. https://doi.org/10.1016/j.ijfatigue.2020.105591

[9] Warhadpande A, Sadeghi F, Evans RD (2013) Microstructural alterations in bearing steels under rolling contact fatigue part 1-historical overview. Tribol Trans 56(3):349–358. https://doi.org/10.1080/10402004.2012.754073

[10] Fu H, Song W, Galindo-Nava EI, Rivera-Díaz-del-Castillo PEJ (2017) Strain-induced martensite decay in bearing steels under rolling contact fatigue: modelling and atomic-scale characterisation. Acta Mater 139:163–173. https://doi.org/10.1016/j.actamat.2017.08.005

[11] Echeverri Restrepo S, Ooi SW, Yan P, Andric P, Vegter RH, Lai J (2021) Dark etching regions under rolling contact fatigue: a review. Mater Sci Technol. https://doi.org/10.1080/02670836.2021.1916252

[12] Jones AB (1946) Metallographic observations of ball bearing fatigue phenomena. In: Symposium on testing of bearings, pp. 35–3518. ASTM International, 100 Barr Harbor Drive, PO Box C700, West Conshohocken, PA 19428-2959. https://doi.org/10.1520/STP42598S . http://www.astm.org/doiLink.cgi?STP42598S

[13] Kuroda M (1960) On the mechanism of flaking due to rolling fatigue of ball and roller bearing steels. Trans Jpn Soc Mech Eng 26(169):1258–1271. https://doi.org/10.1299/kikai1938.26.1258

[14] Merwin JE, Johnson KL (1963) An analysis of plastic deformation in rolling contact. Proceedings of the institution of mechanical engineers 177(1):676–690. https://doi.org/10.1243/PIME_PROC_1963_177_052_02

[15] King AH, O'Brien JL (1965) Microstructural alterations in rolling contact fatigue. In: Advances in electron metallography: Vol. 6, pp. 74–7415. ASTM International, 100 Barr Harbor Drive, PO Box C700, West Conshohocken, PA 19428-2959. https://doi.org/10.1520/STP46420S . http://www.astm.org/doiLink.cgi?STP46420S

[16] Martin JA, Borgese SF, Eberhardt AD (1966) Microstructural alterations of rolling–bearing steel undergoing cyclic stressing. J Basic Eng 88(3):555. https://doi.org/10.1115/1.3645902

[17] Borgese S (1967) An electron fractographic study of spalls formed in rolling contact. J Basic Eng 89(4):943–948. https://doi.org/10.1115/1.3609741

[18] Shiko S, Okamoto K, Watanabe S (1968) Effect of metallographical factors on the rolling fatigue life of ball bearing steel. Tetsu-to-Hagane 54(13):1353–1366. https://doi.org/10.2355/tetsutohagane1955.54.13_1353

[19] Lund T (1969) Structural alterations in fatigue-tested ball-bearing steel. Jernkontorets Annaler 153(7):337–343

[20] Borgese S (1970) A study of the growth mechanism of lenticular carbides in cyclically stressed 52100 steel. J Lubr Technol 92(1):54. https://doi.org/10.1115/1.3451340

[21] Sugino K, Miyamoto K, Nagumo M, Aoki K (1970) Structural alterations of bearing steels under rolling contact fatigue. Trans Iron Steel Instit Jpn 10(2):98–111

[22] Aoki K, Nagumo M, Sugino K (1973) Some metallurgical problems on the life of rolling bearing. Technical Report 2, Nippon Steel

[23] Kang J-H, Hosseinkhani B, Vegter RH, Rivera-Díaz-del-Castillo PEJ (2015) Modelling dislocation assisted tempering during rolling contact fatigue in bearing steels. Int J Fatigue 75:115–125. https://doi.org/10.1016/j.ijfatigue.2015.01.013

[24] Perez M, Sidoroff C, Vincent A, Esnouf C (2009) Microstructural evolution of martensitic 100cr6 bearing steel during tempering: from thermoelectric power measurements to the prediction of dimensional changes. Acta Mater 57(11):3170–3181. https://doi.org/10.1016/j.actamat.2009.03.024

[25] Kuzmann E, Homonnay Z, Klencsár Z, Szalay R (2021) 57Fe Mössbauer spectroscopy as a tool for study of spin states and magnetic interactions in inorganic chemistry. Molecules 26(4):1062. https://doi.org/10.3390/molecules26041062

[26] Myers HP (1997) Introductory solid state physics. CRC Press, Hoboken. https://doi.org/10.1201/9780429320286 . https://www.taylorfrancis.com/books/9781000707625

[27] Klencsár Z (2013) MossWinn–methodological advances in the field of Mössbauer data analysis. Hyperfine Interact 217(1–3):117–126. https://doi.org/10.1007/s10751-012-0732-2

[28] Kaplow R, Ron M, DeCristofaro N (1983) Mössbauer effect studies of tempered martensite. Metall Trans A 14(6):1135–1145. https://doi.org/10.1007/BF02670451

[29] Bruna P, Pradell T, Crespo D, García-Mateo C, Bhadeshia HKDH (2005) Mössbauer analysis of low-temperature bainite. In: AIP conference proceedings, vol. 765, pp. 338–343. AIP, ???. https://doi.org/10.1063/1.1923678 . https://pubs.aip.org/aip/acp/article/765/1/338-343/683592

[30] Pierce DT, Coughlin DR, Williamson DL, Clarke KD, Clarke AJ, Speer JG, De Moor E (2015) Characterization of transition carbides in quench and partitioned steel microstructures by mössbauer spectroscopy and complementary techniques. Acta Materialia 90:417–430. https://doi.org/10.1016/j.actamat.2015.01.024

[31] Liu X-W, Zhao S, Meng Y, Peng Q, Dearden AK, Huo C-F, Yang Y, Li Y-W, Wen X-D (2016) Mössbauer spectroscopy of iron carbides: from prediction to experimental confirmation. Sci Rep 6:26184. https://doi.org/10.1038/srep26184

[32] Ron M, Shechter H, Hirsch AA, Niedzwiedz S (1966) On the mössbauer study of cementite. Phys Lett 20(5):481–483. https://doi.org/10.1016/0031-9163(66)90962-0

[33] Ohki T, Yaguchi H, Maki K, Minamida T, Ibaraki N, Nasu S (1998) Change in the form of cementite in high carbon steel wires. Hyperfine Interact 112(1):147–150

[34] Williamson DL, Nakazawa K, Krauss G (1979) A study of the early stages of tempering in an fe-1.2 pct alloy. Metallurgical Trans A 10:1351–1363

[35] Ino H, Ito T, Nasu S, Gonser U (1982) A study of interstitial atom configuration in fresh and aged iron-carbon martensite by mossbauer spectroscopy. Acta Metall 30(1):9–20. https://doi.org/10.1016/0001-6160(82)90039-6

[36] Sugino K, Miyamoto K, Nagumo M, Aoki K (1970) Structural alterations of bearing steels under rolling contact fatigue. ISIJ Int 10:98–111

[37] Voskamp AP (1985) Material response to rolling contact loading. J Tribol 107(3):359–364. https://doi.org/10.1115/1.3261078